International Journal of Mechanical Sciences 182 (2020) 105725

Contents lists available at ScienceDirect

International Journal of Mechanical Sciences

journal homepage: www.elsevier.com/locate/ijmecsci

Modelling torque and temperature in friction stir welding of aluminium alloys

D.G. Andrade [a,b], C. Leitão [b,*], N. Dialami [c], M. Chiumenti [c], D.M. Rodrigues [a]

[a] ISISE, Mechanical Engineering Department, University of Coimbra, Portugal
[b] CEMMPRE, Mechanical Engineering Department, University of Coimbra, Portugal
[c] Universitat Politècnica de Catalunya, Jordi Girona 1-3, Edifici C1, 08034 Barcelona, Spain, & Centre Internacional de Mètodes Numèrics en Enginyeria (CIMNE), Building C1, Campus Nord UPC, Gran CapitánS/N, 08034 Barcelona, Spain

ARTICLE INFO

Keywords:
FSW
Torque
Temperature
Modelling

ABSTRACT

An analysis of the evolution of the torque and of the temperature with welding conditions, in Friction Stir Welding (FSW) of aluminium alloys, was conducted. More precisely, torque and temperature results from a large number of publications, on FSW of AA2xxx, AA5xxx, AA6xxx and AA7xxx aluminium alloys series, were collected. The literature data was complemented with results from a fully coupled thermomechanical analysis of the FSW welding process. Coupling the experimental data, from the literature, with numerical simulation results, the individual influence of the main process parameters, tools and plates characteristics, on the torque and on the temperatures in FSW was assessed. It was found that the tool rotational speed govern the heat generation, while the tool dimensions have a very important influence, not only on the heat generation but also on the volume of material being stirred during welding, which is another important factor determining the welding torque. The traverse speed and the base material thickness were also found to be important factors governing the torque during welding. However, the influence of the traverse speed on torque evolution is conditioned by the tool dimensions. A parametric analysis enabling to understand the relation between process parameters, heat generation, heat dissipation and base material stirring, was conducted. Analytical relations, which enable calculating the torque and the temperature, in FSW of aluminium alloys, were developed based on numerical results and tested using the data from the literature review.

1. Introduction

The proper application of the Friction Stir Welding (FSW) technique requires the identification of the primary process parameters, i.e. those controlling the heat generation and dissipation, as well as the amount of material flow during welding. Nowadays, since no model relating FSW parameters, machine output data, heat generation and base material stirring during welding is available, any new process application needs to be planned based on trial and error experiments, which according to Magalhães et al. [1] is an important drawback in FSW industrialisation. The development of process control strategies, enabling online quality control, is another critical issue in assisting FSW industrialisation.

Several works analysed the viability of using the tool torque as a process response to the thermomechanical conditions developed during FSW. Longhurst et al. [2] proposed the use of the torque, instead of force, as a process control parameter. According to the authors, the control of the torque allows to produce welds without defects and adapt the weld process to the changes in the surface conditions of the workpiece. Bachmann et al. [3] developed a temperature control system based on an analytical torque model. The authors observed that the welds produced with this control system displayed higher quality and higher homogeneity along the weld length. Leitão et al. [4], in FSW of 5xxx and 6xxx aluminium alloys, also found that when welds without defects were produced, the torque registered during welding could be related to the process parameters, following a well defined empirical relationship. However, when using process parameters conducting to the production of welds with defects, no clear relationship could be established between torque evolution and process parameters, since the torque results were almost aleatory. In the same way, Galvão et al. [5], in dissimilar friction stir welding of aluminium and copper, registered that analysing the torque evolution during welding it is possible to determine the formation of defects resulting from the realising of important quantities of intermetallics from under the tool. Kumar et al. [6] also related the variation of the torque during welding with the formation of surface defects. From all these works, it is possible to conclude that understanding and modelling the influence of process parameters on torque can be

* Corresponding author.
E-mail address: carlos.leitao@dem.uc.pt (C. Leitão).

https://doi.org/10.1016/j.ijmecsci.2020.105725
Received 5 March 2020; Received in revised form 8 April 2020; Accepted 23 April 2020
Available online 16 May 2020

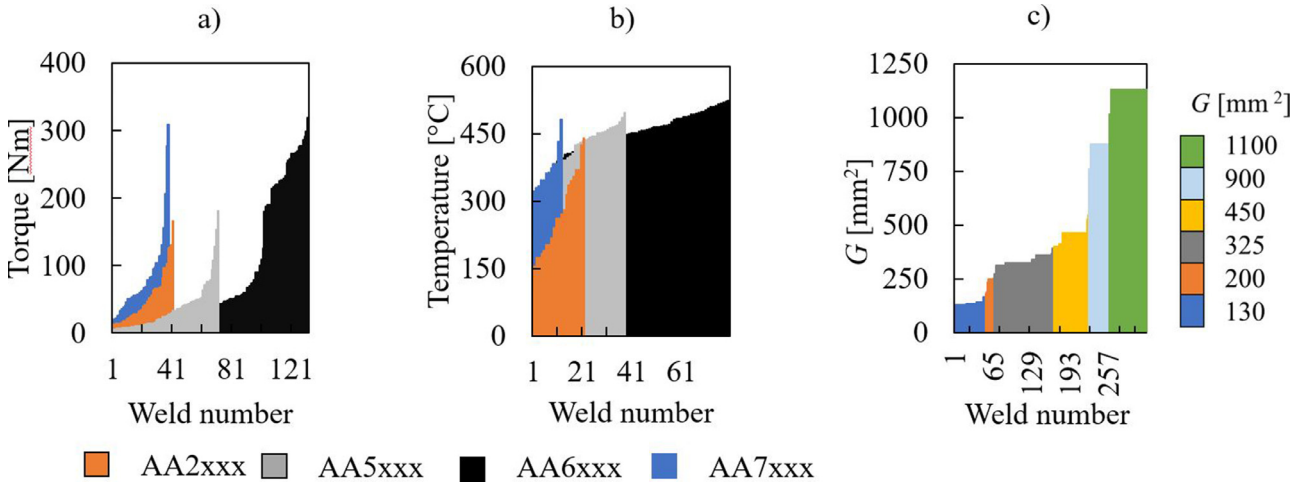

Fig. 1. Range of torque (a), temperature (b) and geometry parameter (c) values covered by the database.

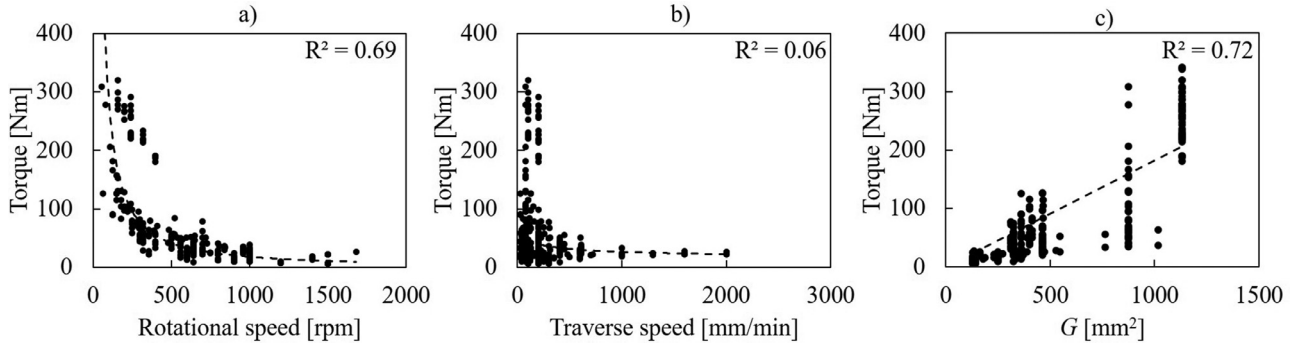

Fig. 2. Evolution of torque with the rotational speed (a), traverse speed (b) and geometry parameter (c). Experimental values from the literature.

an important instrument, not only in selecting process parameters for different applications, but also in controlling the process itself and detecting the formation of welding defects. Other works have also shown the importance of controlling the torque in different production processes such as friction welding [7], rolling [8–10], machining [11,12], among others.

Khandkar et al. [13] and Schmidt et al. [14] proposed the following model

$$M = M_{shoulder} + M_{pin\ surface} + M_{pin\ bottom} \tag{1}$$

$$M = \int_{r_p}^{r_s} (r\tau)2\pi r dr + \left(r_p \tau\right)2\pi r_p p_l + \int_{0}^{r_p} (r\tau)2\pi r dr \tag{2}$$

to predict the torque (M), taking into account the individual contribution of the different tool components and base material properties on the torque values. In the above equations, r is the radial distance from the centre of rotation to the outer edge of the tool shoulder, r_s and r_p are the tool shoulder and pin radius, p_l is the pin length and τ is the shear stress at the tool-base material interface. According to Schmidt et al. [14], the shear stress, which varies according to the contact conditions, i.e. the occurrence of slipping or sticking contact, can be estimated using the equation

$$\tau = (1-\delta)\tau_{plastic} + \delta\tau_{friction} \tag{3}$$

where δ is the slipping fraction, $\tau_{plastic}$ is the shear stress due to the sticking contact and $\tau_{friction}$ is the shear stress due to the slipping contact. The shear associated with the sticking contact is estimated based on the yield stress of the base material (σ_y), using the von Mises yield criterion:

$$\tau_{plastic} = \frac{\sigma_y}{\sqrt{3}}\,. \tag{4}$$

The shear stress associated to the slipping contact is estimated using the Coulomb's friction law,

$$\tau_{friciton} = \mu_f P \tag{5}$$

where P is the contact pressure and μ_f is the friction coefficient between the tool and the workpiece. The previous model requires the knowledge of the slipping fraction and of the friction coefficient, under the thermomechanical conditions imposed by the FSW process, which are very difficult to determine. Those uncertainties lead to the development of other analytical models, relating the torque with process parameters.

Colegrove and Shercliff [15] proposed a model that includes the effect of the traverse (v) and rotational (ω) speeds on the torque, which is given by the equation,

$$M = K\frac{v^{\alpha}}{\omega^{\beta}} \tag{6}$$

where β, α and K are constants. If both α and β are equal to 1, the previous model displays a linear relation between the torque with the welding heat input. Arbegast and Hartley [16] have used this heat index to represent the welding temperature evolution, where α and β were taken has 1 and 2, respectively. However, none of the previous models take explicitly into account the influence of the tool geometry and/or the plate thickness, i.e. the amount of material dragged by the tool, on the torque registered during welding. However, in Colegrove and Shercliff [15] it may be assumed that the influence of those parameters on the torque evolution may be taken into account through the constant K.

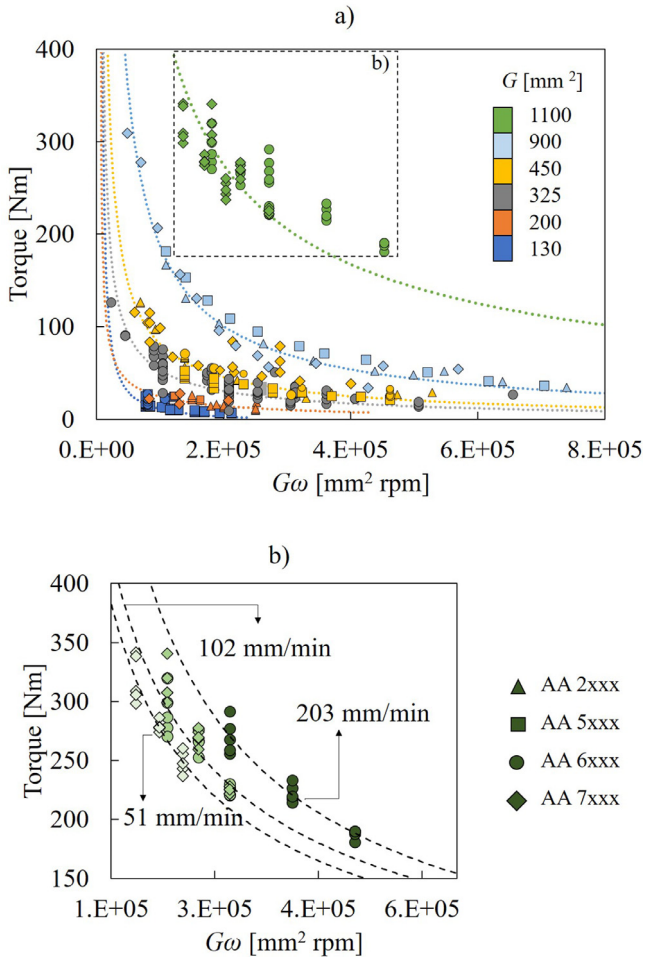

Fig. 3. Evolution of torque with the geometry parameter multiplied by the rotational speed (Gω). Experimental values from the literature.

It is also important to enhance that the Colegrove and Shercliff [15] model can only predict the evolution of the torque with the process parameters if the values of ω and v are kept inside a certain range. For instance, when ω is close to 0, M values become too high, and for high values of ω, M becomes 0. Based on this model limitation, Cui et al. [17] developed an alternative model:

$$M = M_0 + M_f e^{-n\omega}. \tag{7}$$

In the previous equations, M_0 is the minimum torque value for the different traverse speeds, n is a decay parameter and M_f is a pre-exponential parameter. According to this model, the maximum torque value (M_{max}), that occurs when ω is close to 0, do not vary with the rotational and traverse speeds, being determined by the alloy strength at room temperature.

Pew et al. [18] also reported a strong relation between the welding temperature and the welding power, obtained by multiplying the torque by the tool rotational speed. Tello et al. [19] even developed an analytical model correlating the torque with the welding temperature, given by the equation

$$M = \frac{2\pi k \Delta T_w}{\eta \omega K_0} \tag{8}$$

where k is the thermal conductivity of the base material, η is the efficiency of the process, K_0 is the modified Bessel function of the second kind and 0 order and ΔT_w is the difference between the temperature at the shear layer interface and the initial temperature of the base material.

In the present work, experimental values of torque and welding temperatures were collected, for a very large range of experimental conditions, by performing a literature review. The influence of the different FSW process parameters, as well as of the plates thicknesses and tool dimensions, on the torque evolution, was also analysed using numerical simulation. This study allowed to expand the Colegrove and Shercliff [15] model, by adding a larger number of process variables to the equation. In the proposed model, the influence of the tool dimensions, rotational speed, traverse speed and base material thickness, on the stirring volume, welding heat input and torque are taken into account. The analytical equations developed for calculating the torque and welding temperatures in aluminium alloys, were fitted successfully to the very large range of welding conditions obtained from the literature.

2. Experimental data

In order to analyse the influence of the process parameters on the FSW torque and temperature, a literature review was performed and a database containing data from more than 300 different friction stir welding tests, in AA2xxx, AA5xxx, AA6xxx and AA7xxx aluminium alloys, in lap and butt joint configurations, was created. The references used to collect the data are presented in Table 1. The database generated contains not only the tool torque and the maximum welding temperatures (T) registered by the different authors, but also the process parameters, i.e. the rotational and traverse speeds, the pin diameter (D_p), the pin length (p_l) and the shoulder diameter (D_s) used in each work.

In Fig. 1a and b it is represented the range of torque and maximum temperature values obtained from the different authors. It should be noted that the temperature measurement position and/or technique varied according to the different works, which may have important influence on the range of results collected. Analysing these figures, in which the results are grouped according to the base material tested, it is possible to conclude that a larger amount of results were available for the AA5xxx and AA6xxx aluminium alloys, since these alloys series are the most common base materials studied in FSW.

In order to take into account the influence of the tool dimensions on the welding outputs, a geometry parameter (G) was developed

$$G = \frac{\pi}{4} D_p^2 + \pi D_p p_l + \frac{\pi}{4} \left(D_s - D_p\right)^2, \tag{9}$$

which corresponds to the contact area between the tool and the workpiece, as in Khandkar et al. [13] and Schmidt et al. [14]. For complex pin or shoulder geometries, G was calculated assuming an equivalent cylindrical geometry to determine D_p. Analysing the G parameters corresponding to all the tools used by the different authors, which are represented in Fig. 1c, it is possible to conclude that a large range of tool dimensions was tested. More precisely, among the different works, D_p, p_l and D_s varied in the range of 3 to 16 mm, 1 to 12.5 mm and 10 to 35 mm, respectively. Due to the large variety of process parameters and tool dimensions considered in the database, the values registered for M varied in the range of 6 to 320 Nm.

The evolution of the torque with ω, v and G is shown in Fig. 2a to c, respectively. The figure enables to observe that the rotational and traverse speeds tested by the different authors vary in the range of 55 to 1700 rpm and 25 to 2000 mm/min, respectively. The effect of the different process parameters on torque was ranked based on the Pearson correlation coefficient (R^2). From the figure, it is possible to conclude that both the tool dimensions and the tool rotational speed may be statistically related to the torque, while no important relation between the traverse speed with the torque may be inferred. Comparing the evolution of torque with ω and G, it is also possible to conclude that both have a comparable influence on the torque since the Pearson correlation coefficients are similar.

Based on the previous conclusion, the evolution of torque versus the product $G\omega$ was analysed and plotted in Fig. 3a, for each base material. In the figure, each colour identifies different torque evolutions corresponding to different levels of G, established according to Fig. 1c.

Table 1
Experimental works used to construct the database.

AA 2xxx	AA 5xxx	AA 6xxx	AA 7xxx
● Yan et al. [20]	● Peel et al. [21]	● Peel et al. [21]	● Long et al. [22]
● Long et al. [22]	● Long et al. [22]	● Emam and Domiaty [23]	● Emam and Domiaty [23]
● Arora et al. [24]	● Leitão et al. [4]	● Cui et al. [17]	● Upadhyay and Reynolds [25]
● Su et al. [26]	● Quintana and Silveira [27]	● Wade and Reynolds [28]	● Mehta et al. [29]
● Ramanjaneyulu et al. [30]	● Cuellar and Silveira [31]	● Leitão et al. [4]	
	● Costa et al. [32]	● Reza-E-Rabby and Reynolds [33]	
		● Banik et al. [34]	
		● Costa et al. [32]	

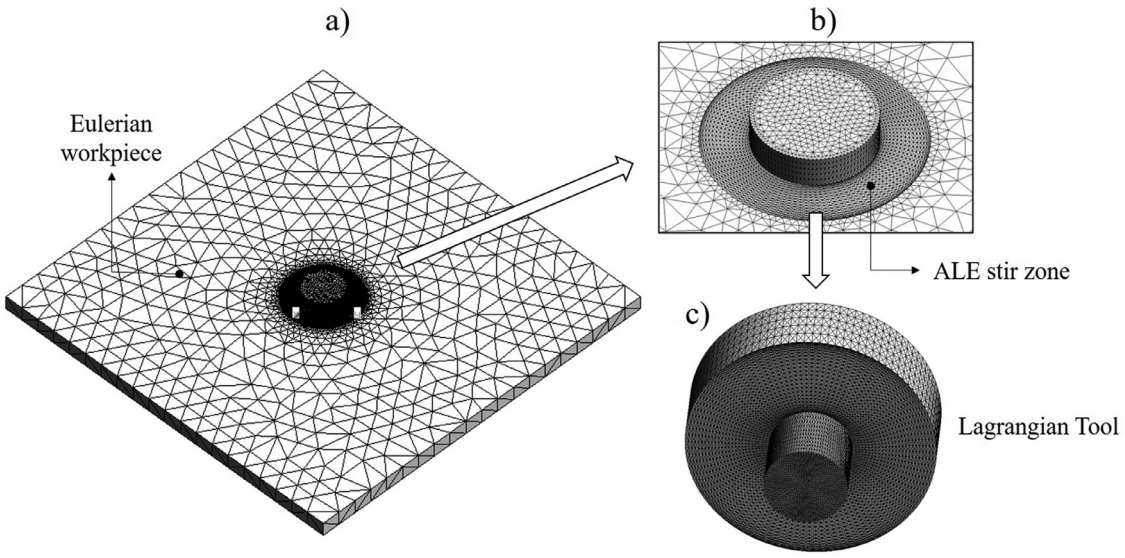

Fig. 4. Finite element model: workpiece geometry (a), stirring zone (b) and tool geometry (c).

Analysing the results, it is possible to conclude that irrespective of the base material welded, the torque results may be divided in different curves/trends in accordance to the tool dimensions (G). For each curve, the torque decreases exponentially with the increase of the rotational speed. However, meanwhile for the lower G values a trend line may be plotted fitting almost accurately the decrease of the torque with ω, for all the materials, for the larger G value (green symbols), an important dispersion of results may be observed. This dispersion is shown in more detail in Fig. 3b, where the different traverse speeds used are identified. Analysing Fig. 3a and b it is possible to conclude that the traverse speed only has important influence on the torque values when tools with large dimensions are used. To the authors knowledge no previous work report the same type of conclusion. In order to understand the influence of G, ω and v on the torque evolution/values, a parametric analysis was conducted using numerical simulation.

3. Numerical simulation

3.1. Numerical model

The welding mechanisms that govern the tool torque and the welding temperatures were studied through numerical simulation of the FSW process. Three sections including the tool, the stir zone and the workpiece were considered in the finite element model. As in Dialami et al. [35–37], an apropos kinematic framework was adopted consolidating three frameworks for the different weld subdomains. Namely, the tool was modelled in a Lagrangian framework and the stir zone and the rest of the workpiece were described using Arbitrary Lagrangian/Eulerian (ALE) and Eulerian frameworks, respectively. The forces acting on the

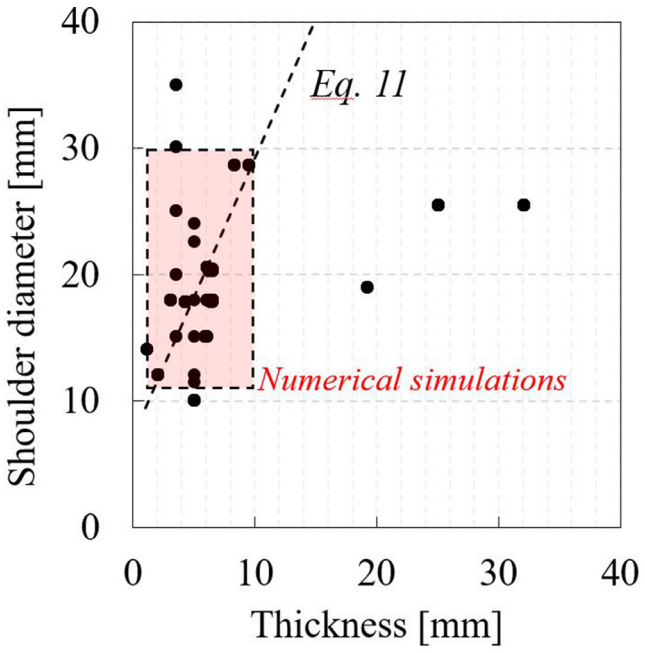

Fig. 5. Tool shoulder diameter versus base material thickness, for all the experimental conditions considered in the database and FE modelling.

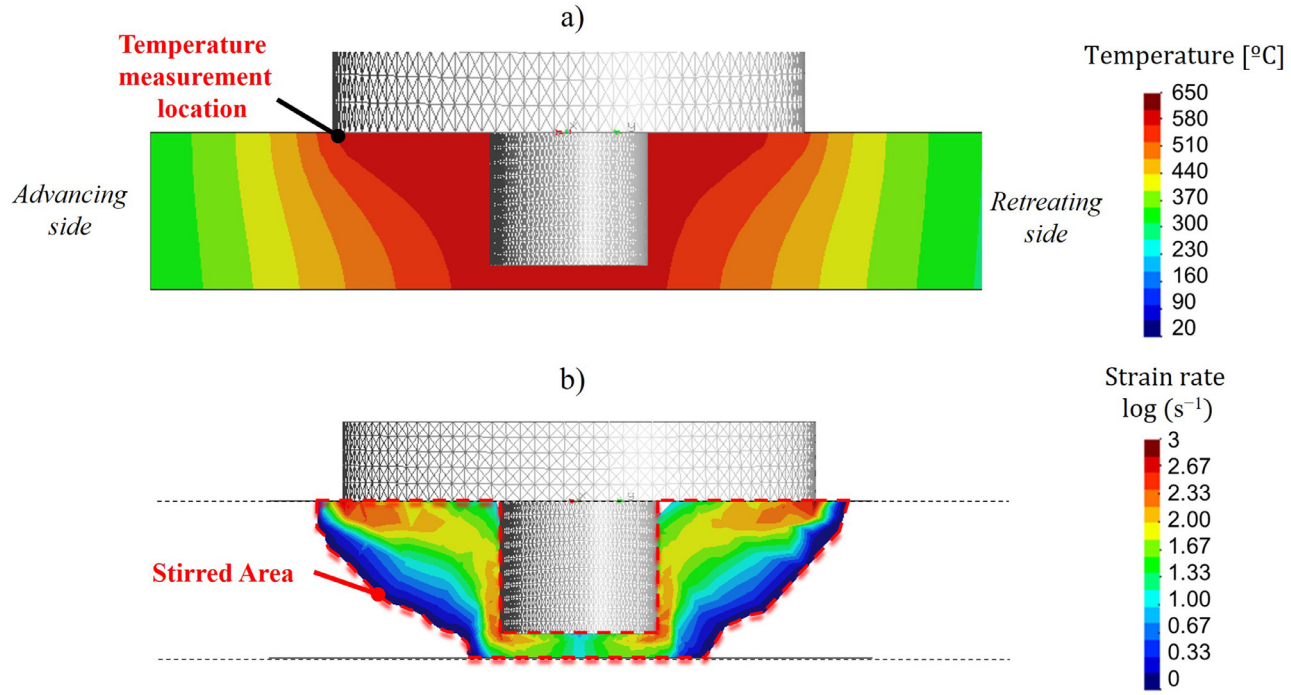

Fig. 6. Distribution maps of temperature (a) and logarithmic equivalent strain rate (b). Results for the weld cross section.

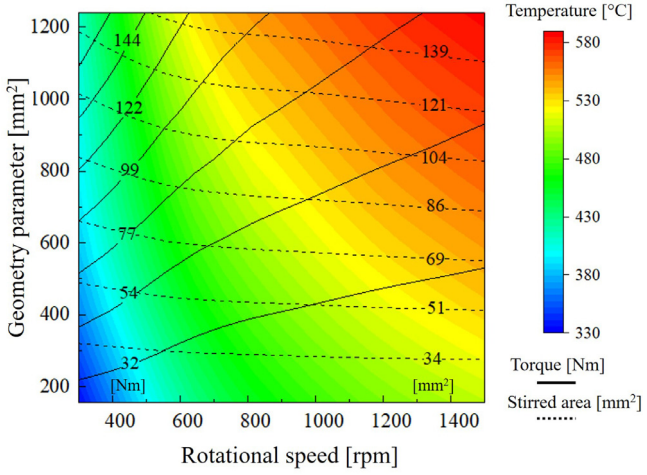

Fig. 7. Numerical results concerning the evolution of the torque, temperature and area of material stirred with the rotational speed and geometry parameter.

tool were calculated by appropriate integration of the tractions at the tool-stirred material interface. In order to save computation time, a fast and accurate two-stage solution strategy was adopted [38]. More precisely, during an initial speed up stage, the steady state solution is calculated by decreasing the thermal capacity of the transient problem. The problem at this phase is defined in a fixed configuration. The periodic stage starts by taking the solution obtained in the first step, as the initial condition, and modelling the movement of the tool. This strategy reduces the FSW simulation time drastically and, at the same time, makes possible the modelling of asymmetrical pin shapes and the visualisation of the material flow during welding. Full sticking contact conditions between the tool and the workpiece were considered in the numerical simulations.

In Fig. 4 is shown the workpiece, the tool geometry and the mesh used in the numerical simulation. The FE mesh contained around 32,000 nodes and 180,000 tetrahedral elements. The base material plates were modelled with 160 mm width and length. The tool was modelled with a cylindrical pin and a flat shoulder. A more refined mesh was used in modelling the tool/workpiece interface, in order to capture the temperature and strain rate gradients. A convection coefficient (h_{conv}) equal to 25 W/m^{2}k and a conduction coefficient (h_{cond}) equal to 1000 W/m^{2}k were used to model the heat exchanges with the surrounding environment and with the backing plate, respectively.

The Norton-Hoff constitutive model was considered to model the base material behaviour,

$$\sigma_{eq}\left(\dot{\varepsilon}_{eq}, T\right)=\sqrt{3}\mu(T)\left(\sqrt{3}\dot{\varepsilon}_{eq}\right)^{m(T)}, \tag{10}$$

where σ_{eq} is the equivalent stress, $\dot{\varepsilon}_{eq}$ the equivalent strain rate and μ (T) and m (T) are the viscosity parameter and exponent, respectively. The base material constitutive properties used in the numerical simulations were taken from Dialami et al. [38]. The remaining governing equations of the numerical model are summarised in Table 2 and the respective nomenclature in Table 3. For a detailed explanation of the computational framework, see Ref. [35–38].

A sensitivity analysis was performed in order to analyse individually the influence of the tool dimensions and of the tool rotational and traverse speeds on the torque and temperature evolution during welding. In the numerical simulations, the tool rotational and traverse speeds were varied in the same range of the welding speeds used in the literature analysed (shown in Figs. 1a and b), i.e. ω was varied between 300 and 1500 rpm and v was varied between 250 and 2000 mm/min. The tool dimensions were also selected based on the experimental works using the data in Fig. 5, where are plotted the shoulder diameters and the base material thicknesses (t) for the welding conditions covered by the database. In the figure, it is also plotted, by a dashed line, the shoulder

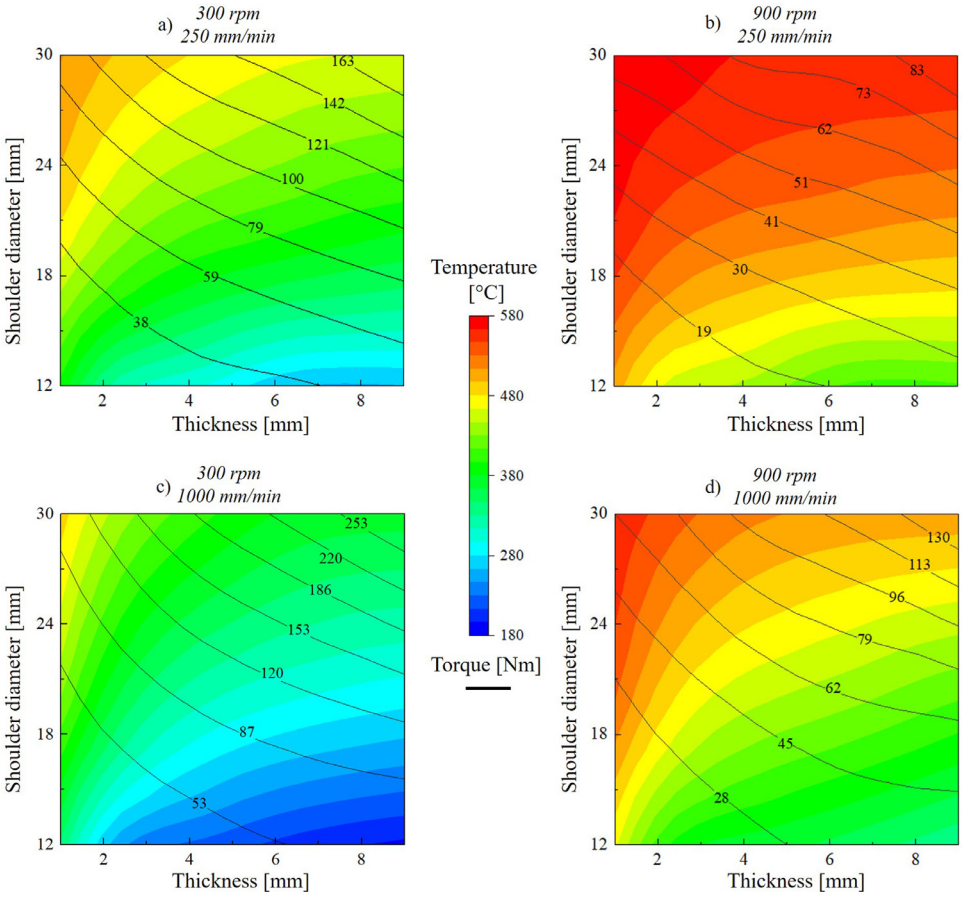

Fig. 8. Numerical results concerning the evolution of torque and temperature with the shoulder diameter and thickness, for rotational and traverse speeds of 300 to 900 rpm and 250 to 1000 mm/min, respectively.

Table 2
Thermo-mechanical formulation.

Mechanical partition	
$\nabla \bullet s + \nabla p + \rho_o b = 0$	Momentum balance equation
$\nabla \bullet \mathrm{v} = 0$	Continuity equation
$\dot{\epsilon} = \nabla^s \mathrm{v}$	Kinematic equation
$\sigma_{eq} = \sqrt{3/2}(s : s)^{1/2}$	Equivalent stress
$\dot{\epsilon}_{eq} = \sqrt{2/3}(\dot{\epsilon} : \dot{\epsilon})^{1/2}$	Equivalent strain rate
Thermal partition	
$\rho_0 c(\frac{1}{\xi}\frac{dT}{dt} + (\mathrm{v} - \mathrm{v}_{mesh}) \cdot \nabla T) - \nabla \cdot (k \nabla T) = D_{mesh}$	Energy balance equation
$D_{mesh} = \theta s : \dot{\epsilon}$	Viscoplastic dissipation
$q_{conv} = h(T - T_{env})$	Heat convection
$q_{cond} = h_{cond}(T - T_{tool})$	Heat conduction

Table 3
Nomenclature.

s	Stress deviator
p	Pressure
ρ_0	Density in the reference configuration
b	Body forces vector per unit of mass
v	Velocity field
$\dot{\epsilon}$	Strain rate
μ	Viscosity parameter
m	Viscosity exponent
c	Specific heat
T	Temperature
v_{mesh}	Velocity of the mesh
k	Thermal conductivity
θ	Fraction of plastic dissipation
h_{conv}	Heat transfer coefficient by convection
h_{cond}	Heat transfer coefficient by conduction
ξ	Speed-up factor
T_{env}	Environmental temperature
T_{tool}	Tool temperature

diameter to plate thickness ratios recommended by Zhang et al. [39],

$$D_s = 2.2t + 7.3 \quad (11)$$

for obtaining non-defective welds. The range of tool dimensions used in the numerical simulations, which are represented in the figure by the red box, were defined in order to consider two situations: (1) shoulder diameters proportional to the plate thickness, calculated using Eq. (11), and (2) constant shoulder diameters and varying plate thicknesses. The pin dimensions were established using a D_s/D_p ratio of 3, as recommended by Prado et al. [40], and a p_l/t ratio of 0.85. This way, the thickness of the base material and the shoulder diameter were varied between 1 and 10 mm and 12 to 30 mm, respectively.

3.2. Numerical results

The influence of the different welding parameters on the torque evolution during welding was analysed by measuring the maximum welding temperatures (T) and the amount of material stirred by the tool, quantified by the stirred area (SA), and relating it to the average torque registered in the numerical simulation. The procedures used to quantify T and SA are exemplified in Fig. 6a and b, where it is shown the temperature and the logarithmic equivalent strain rate distribution, respectively, in the weld cross section, when steady-state conditions are

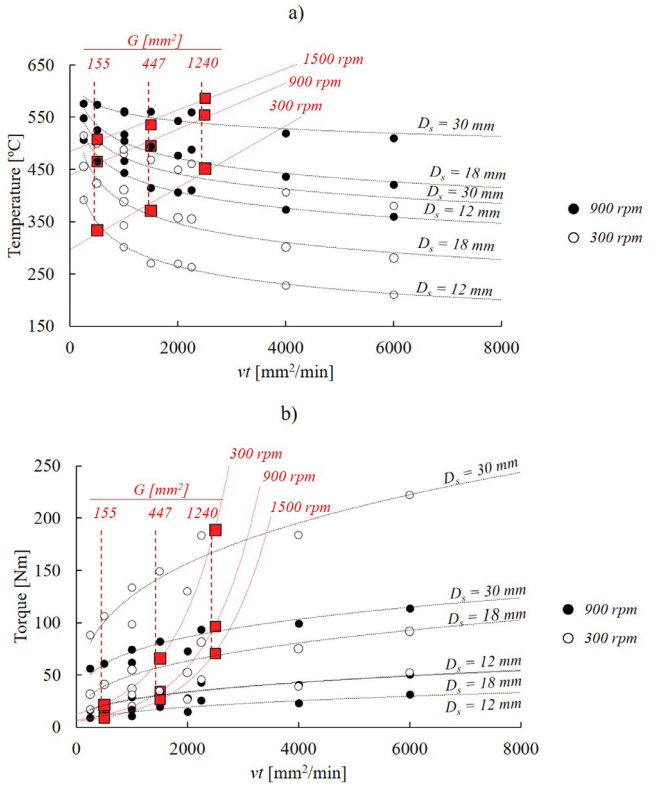

Fig. 9. Evolution of temperature (a) and torque (b) with the traverse speed multiplied by the plate thickness (vt) when heat dissipative effects are minimized (red squares) and maximized (black circles).

reached during welding. As shown in Fig. 6a the temperature distribution in the welds was asymmetrical, with maximum temperatures registered at the advancing side of the weld. The temperatures used in the analysis were measured in a point located at the outer shoulder radius, at the advancing side of the tool. The amount of material stirred by the tool was evaluated by measuring the area of material with equivalent strain rate higher than zero, as shown in Fig. 6b.

In Fig. 7 is shown the evolution of the welding torque (continuous lines) with ω and G. The results were obtained by varying ω between 300 and 1500 rpm and using a constant welding speed of 250 mm/min. The G values were set assuming a proportionality between the shoulder diameter and the plates thickness, i.e. using Eq. (11) for calculating the shoulder diameter and assuming plate thicknesses varying between 2 and 10 mm. Analysing the figure, it is possible to conclude that, in accordance to the experimental results, for constant tool rotational speeds, the torque registered in the numerical simulations increased with G, and for constant G values, the torque decreased with increasing ω. However, the figure also shows that the influence of G on the torque evolution is more significant for low than for high rotational speeds and, on the other hand, the influence of the rotational speed on the torque evolution is more significant for large than for low values of G.

The evolution of the torque with ω and G may be explained analysing the evolution of the maximum welding temperatures (coloured map) and of the stirred area (dashed lines) with the process parameters. The colour map in Fig. 7 shows that the welding temperatures increase with the tool rotational speed, irrespective of the tool dimensions, and stabilise in maximum values for large values of ω and G. The stabilisation of the maximum temperature corresponds to the threshold in heat generation which is known to prevent the welding temperature from reaching the base material melting temperature, ensuring solid-state welding in FSW irrespective of the welding parameters. However, meanwhile for low values of G, the decrease of the torque with ω, reported in the previous paragraph, may be attributed to the base material softening with increasing temperatures, for high G values the same is not true, since high torque values were registered in the very high temperature domain. Therefore, the increase in the torque with G has to be related to the increase of the amount of material stirred by the tool. Analysing Fig. 7 it is possible to confirm that, independent of ω, the stirred area increases with G, i.e. with increasing tool dimensions and plate thickness. The only exception is in the very high temperature domain, where a gradual decrease in the stirred area with increasing ω may be observed.

In Fig. 8 is now shown the evolution of the torque (continuous lines) with the shoulder diameter and thickness for two different values of rotational speed (300 and 900 rpm) and two different values of traverse speed (250 and 1000 mm/min). In these numerical simulations, no proportionality between the tool dimensions and plate thickness was assumed, i.e. in each simulation the D_s/t ratio was not set according to Eq. (11), being selected in order to cover the full range of tool dimensions highlighted by the red shaded area in Fig. 5. As shown in Fig. 8, tools with shoulder diameters varying from 12 to 30 mm were tested for the welding of 1 to 9 mm thick plates. Analysing the torque results it is possible to conclude that, irrespective of ω and v, the larger torque values were always registered for the simulations corresponding to the tools with the larger shoulder diameter and the larger thicknesses, i.e. for the larger G values, which is in accordance with the experimental results. Comparing the four plots, it is also possible to conclude that for the same range of shoulder diameters and plate thicknesses, the torque values were higher in the simulations performed with the lower tool rotational speed and/or the higher traverse speed.

Analysing in Fig. 8 the evolution of the temperature (coloured maps) with process parameters it is possible to conclude that the welding temperatures were higher in the numerical simulations performed with the higher tool rotational speed of 900 rpm and the higher shoulder diameters. Comparing the temperature values in Fig. 8a and b and Fig. 8c and d it is even possible to conclude that heat generation was determined by the tool rotation, in first, and by the shoulder diameter, in second. On the other hand, the evolution of the temperatures in each graph also enables to conclude that for constant shoulder diameters, the temperature decreases with increasing plate thicknesses. In the same way, the differences in temperature fields between Fig. 8a and c and Fig. 8b and d, also enable to conclude that irrespective of D_s and ω, the temperatures decrease when increasing the traverse speed. Those results point for the strong influence of v and t on the welding temperature, indicating that these parameters should also be considered in the modelling of the torque evolution with process parameters. However, these results also enhance that the influence of v on the torque and temperature is more pronounced for welding conditions corresponding to large G values, as already stressed when analysing the results in Fig. 3b.

4. Modelling torque and temperature

Fig. 9a and b show the evolution of the temperature and torque, respectively, versus the product of the traverse speed by the plate thickness (vt). Both parameters were found to be important factors in determining the welding heat dissipation in the previous analysis. In the figure, the results plotted with red squares correspond to the numerical simulations of Fig. 7, in which heat dissipative effects associated with the thickness and the traverse speed were minimised by assuming a constant value for v and setting the shoulder diameter proportional to the plates thickness. The results plotted with circles correspond to the numerical simulations of Fig. 8, in which the shoulder diameters, plate thicknesses and traverse speeds were selected in order to enhance the heat dissipative effects on the temperature fields.

Analysing Fig. 9a, it is possible to conclude that the welding temperature increases with G and ω, which were found as the main factors in heat generation in the previous analysis, but decrease non-linearly with

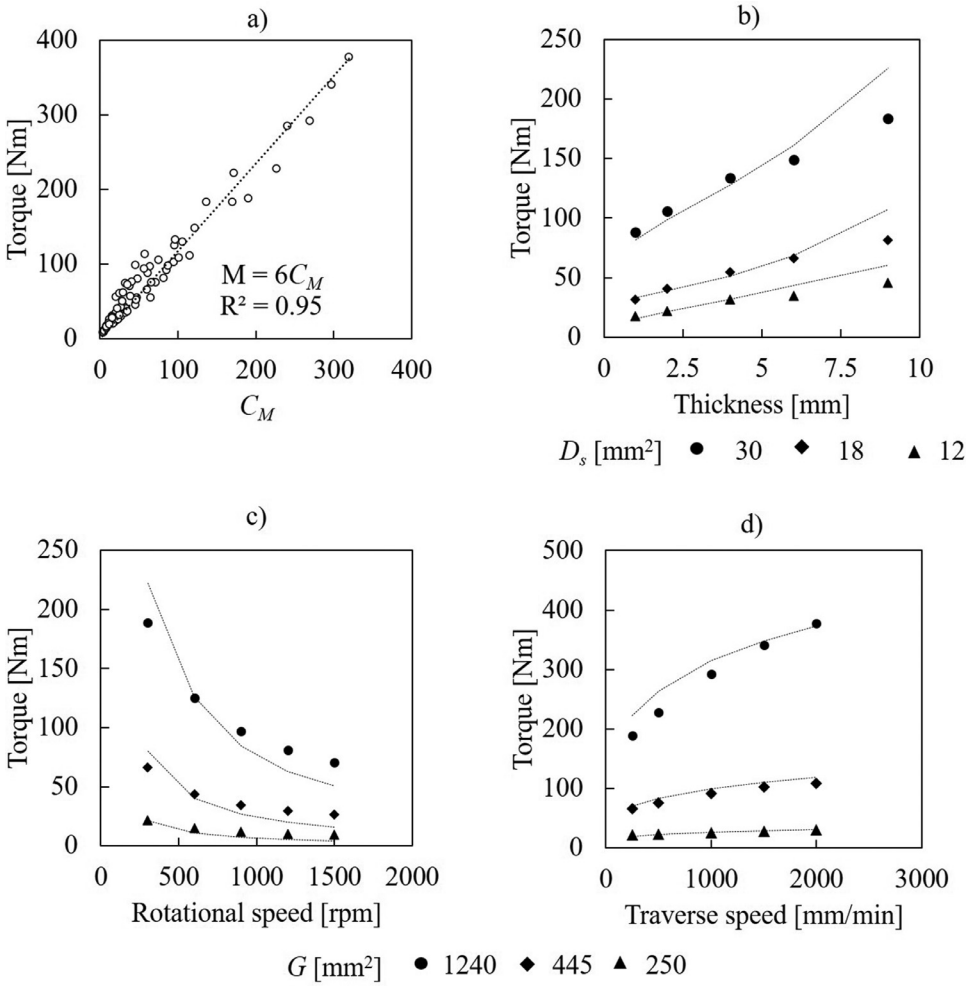

Fig. 10. Evolution of the torque values, obtained in the numerical simulations, with the torque coefficient (a). Comparison between the torque values, obtained in the numerical simulations, for different plate thicknesses (b), rotational speeds (c) and traverse speeds (d) with the torque values calculated with Eq. (14) (dashed lines).

the *vt* product. Analysing now the evolution of the torque in Fig. 9b, it is possible to conclude that the torque decreases with ω, which is the main factor in heat generation, but increases with G, which is the main factor in determining the volume of material stirred by the tool. The torque also increases non-linearly with the product (vt), due to the important influence of both parameters in heat dissipation, i.e. in decreasing the welding temperature.

From the results in Fig. 9, two coefficients, relating the heat generation and the volume of stirred material, governed by ω and G, respectively, and the heat dissipation, governed by v and t, are proposed to be used in quantifying the average torque and the maximum temperature attained during welding. The torque (C_M) and temperature (C_T) coefficients are given by

$$C_M = \frac{G}{\omega}\sqrt[4]{vt}, \tag{12}$$

and,

$$C_T = \frac{G\omega}{\sqrt{vt}}. \tag{13}$$

Assuming $\alpha = \frac{1}{4}$ and $K = G\sqrt[4]{t}$, these coefficients resembles Colegrove and Shercliff [15] model for torque. However, a larger number of process parameters, enabling to better describe the welding conditions in use, is taken into account in the proposed coefficients. In Fig. 10 a are plotted the torque values obtained in the numerical simulations performed in current work versus the torque coefficient C_M. Based on the figure, it is possible to establish a linear relationship between the torque and C_M

$$M = K_M \frac{G}{\omega}\sqrt[4]{vt}. \tag{14}$$

In this equation, a new constant K_M is introduced, which resembles the M_{max} in Cui et al. [17] model. According to this author, M_{max} is determined by the strength of the base materials at room temperature. According to present authors, K_M is determined by the plastic properties of the alloy being welded, which were already found to determine the weldability in FSW of aluminium alloys in a previous work [41]. For the aluminium alloy tested in the numerical simulation work, fitting the numerical results it was determined that $K_M = 6$. The torque values obtained from Eq. (14) are compared to the torque values obtained in the numerical simulations in Fig. 10b to d. In these figures, the torque results are plotted versus the plate thickness (Fig. 10b), the rotational speed (Fig. 10c) and the traverse speed (Fig. 10d). All the figures show that the proposed model satisfactorily reflects the evolution of the average torque with process parameters.

In Fig. 11 the model previsions are now compared with some of the experimental results from the database. Since different aluminium alloys were used by the different authors, and K_M is a material property related parameter, its value had to be adjusted according to the base material in use in each reference. Analysing the figure, it is possible to conclude that the C_M coefficient is able to reproduce satisfactorily the torque evolution for the experimental welding conditions covered by the database.

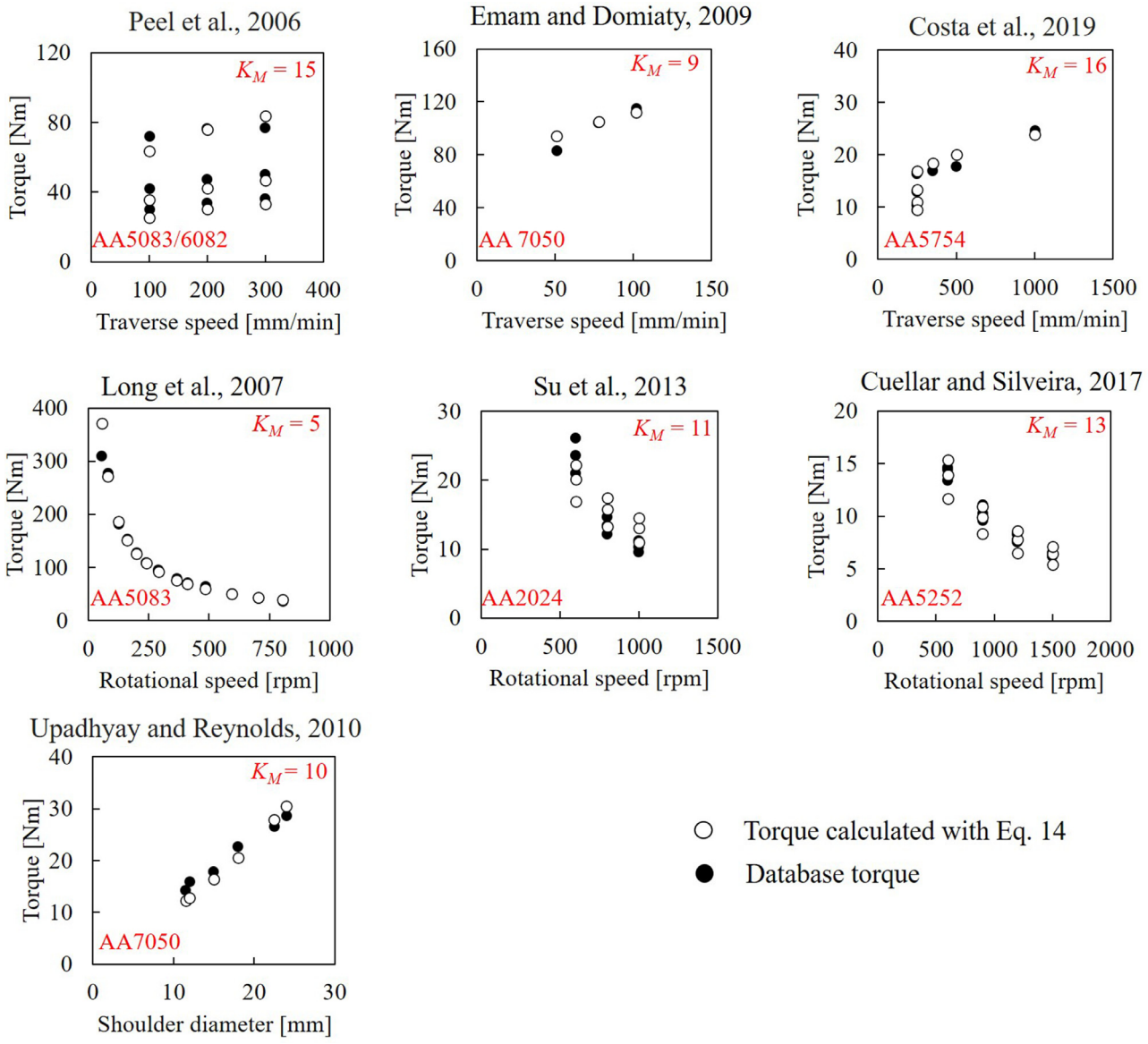

Fig. 11. Comparison of the experimental torque results, from the database, with the torque values calculated with Eq. (14).

In Fig. 12 are now plotted the maximum welding temperatures, obtained in the numerical simulations, versus the temperature coefficient C_T. The figure clearly shows that for C_T higher than 20,000, the maximum welding temperatures remain constant, indicating that this value of C_T may be considered as a heat generation threshold indicator for aluminium alloys. As was done for the torque, the C_T coefficient was correlated with the temperature values, being obtained an equation to predict the welding temperature. So, according to the figure, the temperatures in FSW of aluminium alloys may be estimated as follows:

$$\begin{cases} T = K_T C_T^{\varphi} \text{ for } C_T < 20000, \\ T = 590°C \text{ for } C_T \geq 20000. \end{cases} \tag{15}$$

In this case, K_T and φ are related to the base material properties that determine heat generation and dissipation. From the numerical simulation results it was determined that $K_T = 50$ and $\varphi = 0.25$.

In Fig. 13, the temperature values previewed by the model are compared with the experimental results from the database. In order to fit accurately the experimental results, the temperature values computed using Eq. (15) and making $K_T = 50$ and $\varphi = 0.25$, had to be multiplied by a λ constant. The need for this constant may be associated with important influence of the different experimental techniques, followed by the different authors, in acquiring the maximum temperature, i.e. differences in temperature measurement techniques, differences in the position at which the temperature was measured relative to the weld axis, or even, differences in the backing plate material, among others. Therefore, λ factors were determined individually for each one of the experimental works, due to the strong dependence of the maximum temperatures registered from the experimental apparatus. However, it is important to enhance that no adjustment in K_T and φ parameters was necessary, indicating that these parameters are constant for all aluminium alloys. In fact, analysing Fig. 13, it is possible to see that despite the different welding conditions, i.e. different shoulder diameters, traverse and rotational speeds, the temperature values computed through C_T always follow the temperature results obtained by the different authors.

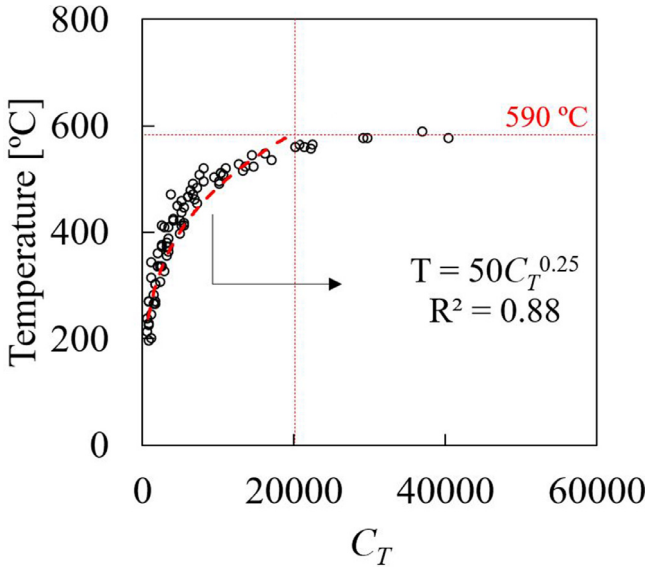

Fig. 12. Evolution of the maximum welding temperatures, obtained in the numerical simulations, with the temperature coefficient.

5. Conclusions

In the present work, the influence of the process parameters, tool dimensions and plate thickness on the torque and welding temperatures was analysed. The main findings of the investigation may be summarized as follows:

- Analytical coefficients (C_M and C_T) were determined for calculating the average torque and the maximum temperature as a function of the welding parameters. The proposed analytical coefficients were validated using experimental results from the literature.
- The tool dimensions and the rotational speed have strong influence on torque and temperature. The proposed coefficients enable to quantify their influence on torque and temperature.
- The traverse speed and the base material thickness are secondary parameters governing the torque and temperature. Their influence on torque is only noticeable when large shoulder tools are used and/or in thick plates welding.
- C_M and C_T coefficients enable to quantify the influence of the traverse speed and plates thickness on torque and temperature.
- The temperature coefficient C_T enables to determine a threshold in the heat generation in FSW, i.e. for C_T>20,000 no temperature increase is expected by changing the welding parameters/conditions.

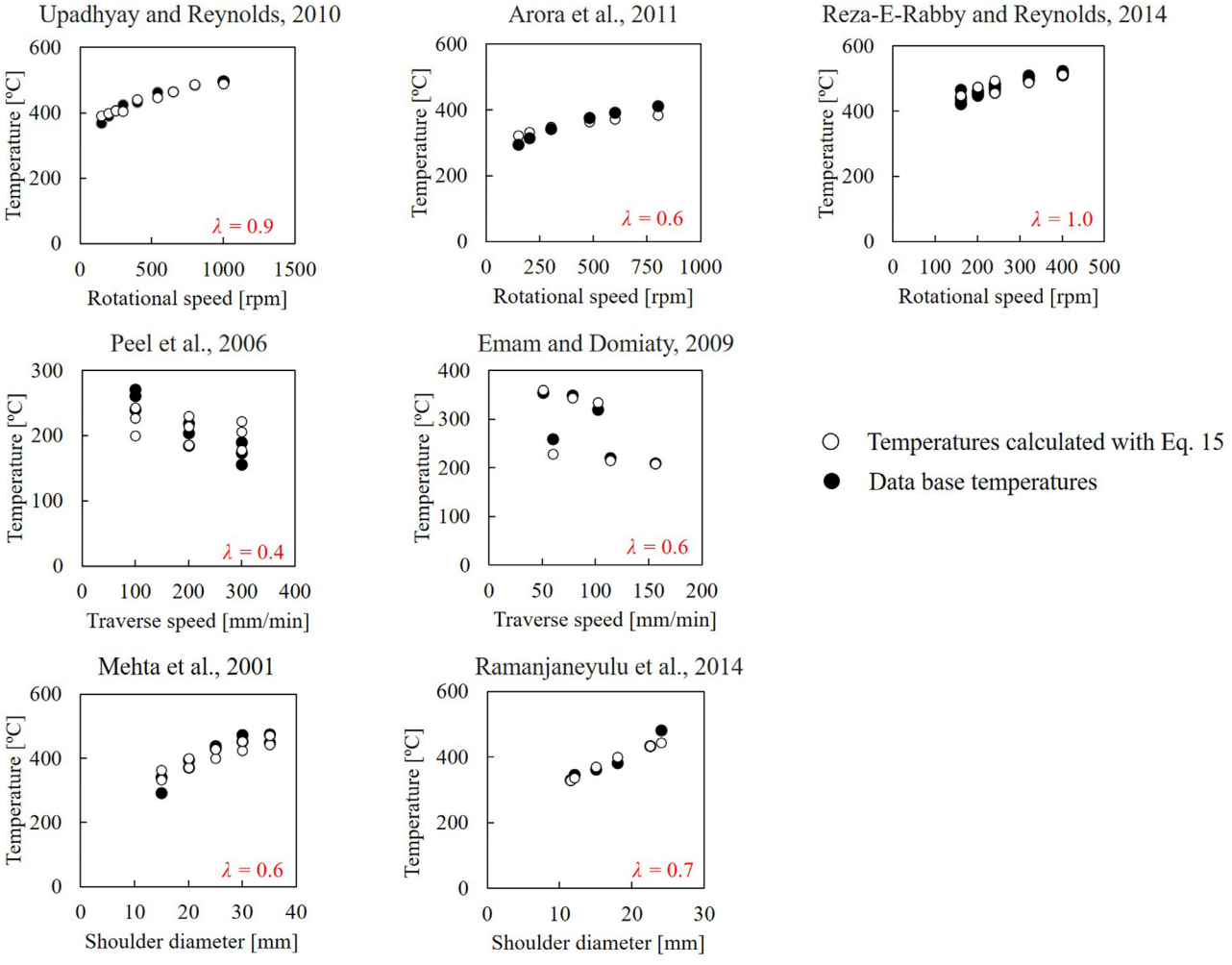

Fig. 13. Comparison between the experimental temperature values, from the database, with the temperature values calculated with Eq. (15).

Declaration of Competing Interest

The authors declare that they have no known competing financial interests or personal relationships that could have appeared to influence the work reported in this paper.

CRediT authorship contribution statement

D.G. Andrade: Conceptualization, Validation, Writing - original draft. **C. Leitão:** Conceptualization, Validation, Writing - original draft. **N. Dialami:** Software, Resources. **M. Chiumenti:** Software, Resources. **D.M. Rodrigues:** Supervision, Conceptualization, Validation, Writing - original draft.

Acknowledgements

This research is sponsored by FEDER funds through Portugal 2020 (PT2020), by the Competitiveness and Internationalization Operational Program (COMPETE 2020) and national funds through the Portuguese Foundation for Science and Technology, under the projects: UID/EMS/00285/2020, POCI-01-0145-FEDER-00763 and Friction 4.0(POCI-01-0145-FEDER-032089). The author, D.G. Andrade is supported by the Portuguese Foundation for Science and Technology through SFRH/BD/130196/2017 fellowship. All supports are gratefully acknowledged.

References

[1] Magalhães VM, Leitão C, Rodrigues DM. Friction stir welding industrialisation and research status. Sci Technol Weld Join 2018;23:400–9. doi:10.1080/13621718.2017.1403110.
[2] Longhurst WR, Strauss AM, Cook GE, Fleming PA. Torque control of friction stir welding for manufacturing and automation. Int J Adv Manuf Technol 2010;51:905–13. doi:10.1007/s00170-010-2678-3.
[3] Bachmann A, Gamper J, Krutzlinger M, Zens A, Zaeh MF. Adaptive model-based temperature control in friction stir welding. Int J Adv Manuf Technol 2017;93:1157–71. doi:10.1007/s00170-017-0594-5.
[4] Leitão C, Louro R, Rodrigues DM. Using torque sensitivity analysis in accessing Friction Stir Welding/Processing conditions. J Mater Process Technol 2012;212:2051–7. doi:10.1016/j.jmatprotec.2012.05.009.
[5] Galvão I, Leitão C, Loureiro A, Rodrigues DM. Study of the welding conditions during similar and dissimilar aluminium and copper welding based on torque sensitivity analysis. Mater Des 2012;42:259–64. doi:10.1016/j.matdes.2012.05.058.
[6] Kumar U, Yadav I, Kumari S, Kumari K, Ranjan N, Kesharwani RK, et al. Defect identification in friction stir welding using discrete wavelet analysis. Adv Eng Softw 2015;85:43–50. doi:10.1016/j.advengsoft.2015.02.001.
[7] Jin F, Li J, Liu P, Nan X, Li X, Xiong J, et al. Friction coefficient model and joint formation in rotary friction welding. J Manuf Process 2019;46:286–97. https://doi.org/10.1016/j.jmapro.2019.09.008.
[8] Duan X, Sheppard T. Three dimensional thermal mechanical coupled simulation during hot rolling of aluminium alloy 3003. Int J Mech Sci 2002;44:2155–72. https://doi.org/10.1016/S0020-7403(02)00164-9.
[9] Shi J, McElwain DLS, Langlands TAM. A comparison of methods to estimate the roll torque in thin strip rolling. Int J Mech Sci 2001;43:611–30. https://doi.org/10.1016/S0020-7403(00)00049-7.
[10] Zhang SH, Zhao DW, Gao CR. The calculation of roll torque and roll separating force for broadside rolling by stream function method. Int J Mech Sci 2012;57:74–8. https://doi.org/10.1016/j.ijmecsci.2012.02.006.
[11] Oezkaya E, Biermann D. Segmented and mathematical model for 3D FEM tapping simulation to predict the relative torque before tool production. Int J Mech Sci 2017;128–129:695–708. https://doi.org/10.1016/j.ijmecsci.2017.04.011.
[12] Lu S, Gao H, Bao Y, Xu Q. A model for force prediction in grinding holes of SiCp/Al composites. Int J Mech Sci 2019;160:1–14. https://doi.org/10.1016/j.ijmecsci.2019.06.025.
[13] Khandkar MZH, Khan JA, Reynolds AP. Prediction of temperature distribution and thermal history during friction stir welding: input torque based model. Sci Technol Weld Join 2003;8(3):165–74.
[14] Schmidt H, Hattel J, Wert J. An analytical model for the heat generation in friction stir welding. Model Simul Mater Sci Eng 2003;12:143–57. doi:10.1088/0965-0393/12/1/013.
[15] Colegrove PA, Shercliff HR. Experimental and numerical analysis of aluminium alloy 7075-T7351 friction stir welds. Sci Technol Weld Join 2003;8:360–8. doi:10.1179/136217103225005534.
[16] Arbegast WJ, Hartley PJ. Friction stir weld technology development at Lockheed Martin Michoud Space System–an overview. ASM Int Trends Weld Res 1999:541–6.
[17] Cui S, Chen ZW, Robson JD. A model relating tool torque and its associated power and specific energy to rotation and forward speeds during friction stir welding/processing. Int J Mach Tools Manuf 2010;50:1023–30. doi:10.1016/j.ijmachtools.2010.09.005.
[18] Pew JW, Nelson TW, Sorensen CD. Torque based weld power model for friction stir welding. Sci Technol Weld Join 2007;12:341–7. doi:10.1179/174329307X197601.
[19] Tello K, Duman U, Mendez P. Scaling laws for the welding arc, weld penetration and friction stir welding. Proc. Eighth Trends Weld. Res. 2009:172–81.
[20] Yan J, Sutton MA, Reynolds AP. Process–structure–property relationships for nugget and heat affected zone regions of AA2524–T351 friction stir welds. Sci Technol Weld Join 2005;10:725–36. doi:10.1179/174329305X68778.
[21] Peel MJ, Steuwer A, Withers PJ, Dickerson T, Shi Q, Shercliff H. Dissimilar friction stir welds in AA5083-AA6082. Part I: process parameter effects on thermal history and weld properties. Metall Mater Trans A Phys Metall Mater Sci 2006;37:2183–93. doi:10.1007/BF02586138.
[22] Long T, Tang W, Reynolds AP. Process response parameter relationships in aluminium alloy friction stir welds. Sci Technol Weld Join 2007;12:311–17. doi:10.1179/174329307X197566.
[23] Emam SA, Domiaty AEl. A refined energy-based model for friction-stir welding. World Acad Sci Eng Technol 2009;29:1010–16.
[24] Arora A, De A, Debroy T. Toward optimum friction stir welding tool shoulder diameter. Scr Mater 2011;64:9–12. doi:10.1016/j.scriptamat.2010.08.052.
[25] Upadhyay P, Reynolds AP. Effects of thermal boundary conditions in friction stir welded AA7050-T7 sheets. Mater Sci Eng A 2010;527:1537–43. doi:10.1016/j.msea.2009.10.039.
[26] Su H, Wu CS, Pittner A, Rethmeier M. Simultaneous measurement of tool torque, traverse force and axial force in friction stir welding. J Manuf Process 2013;15:495–500. doi:10.1016/j.jmapro.2013.09.001.
[27] Quintana KJ, Silveira JLL. Mechanistic models and experimental analysis for the torque in FSW considering the tool geometry and the process velocities. J Manuf Process 2017;30:406–17. doi:10.1016/j.jmapro.2017.09.031.
[28] Wade M, Reynolds AP. Friction stir weld nugget temperature asymmetry. Sci Technol Weld Join 2010;15:64–9. doi:10.1179/136217109X12562846839150.
[29] Mehta M, Arora A, De A, DebRoy T. Tool geometry for friction stir welding-optimum shoulder diameter. Metall Mater Trans A 2011;42:2716–22. doi:10.1007/s11661-011-0672-5.
[30] Ramanjaneyulu K, Madhusudhan Reddy G, Venugopal Rao A. Role of tool shoulder diameter in friction stir welding: an analysis of the temperature and plastic deformation of AA 2014 aluminium alloy. Trans Indian Inst Met 2014;67:769–80. doi:10.1007/s12666-014-0401-z.
[31] Cuellar, Quintana Karen Johanna, Silveira JLL. Analysis of torque in friction stir welding of aluminum alloy 5052 by inverse problem method. J Manuf Sci Eng 2017;139:41017–18.
[32] Costa MI, Leitão C, Rodrigues DM. Parametric study of friction stir welding induced distortion in thin aluminium alloy plates: a coupled numerical and experimental analysis. Thin-Walled Struct 2019;134:268–76. https://doi.org/10.1016/j.tws.2018.10.027.
[33] Reza-E-rabby M, Reynolds AP. Effect of tool pin thread forms on friction stir weldability of different aluminum alloys. Procedia Eng 2014;90:637–42. doi:10.1016/j.proeng.2014.11.784.
[34] Banik A, Saha Roy B, Deb Barma J, Saha SC. An experimental investigation of torque and force generation for varying tool tilt angles and their effects on microstructure and mechanical properties: friction stir welding of AA 6061-T6. J Manuf Process 2018;31:395–404. doi:10.1016/j.jmapro.2017.11.030.
[35] Dialami N, Chiumenti M, Cervera M, Agelet de Saracibar C. An apropos kinematic framework for the numerical modeling of friction stir welding. Comput Struct 2013;117:48–57. https://doi.org/10.1016/j.compstruc.2012.12.006.
[36] Dialami N, Chiumenti M, Cervera M, Segatori A, Osikowicz W. Enhanced friction model for Friction Stir Welding (FSW) analysis: simulation and experimental validation. Int J Mech Sci 2017;133:555–67. https://doi.org/10.1016/j.ijmecsci.2017.09.022.
[37] Dialami N, Cervera M, Chiumenti M, Segatori A. Prediction of joint line remnant defect in friction stir welding. Int J Mech Sci 2019;151:61–9. https://doi.org/10.1016/j.ijmecsci.2018.11.012.
[38] Dialami N, Cervera M, Chiumenti M, de Saracibar CA, Agelet de Saracibar C, de Saracibar CA, et al. A fast and accurate two-stage strategy to evaluate the effect of the pin tool profile on metal flow, torque and forces in friction stir welding. Int J Mech Sci 2017;122:215–27. doi:10.1016/j.ijmecsci.2016.12.016.
[39] Zhang YN, Cao X, Larose S, Wanjara P. Review of tools for friction stir welding and processing. Can Metall Q 2012;51:250–61. doi:10.1179/1879139512Y.0000000015.
[40] Prado RA, Murr LE, Shindo DJ, Soto KF. Tool wear in the friction-stir welding of aluminum alloy 6061+20 Al 2 O 3 : a preliminary study. Scr Mater 2001;45:75–80.
[41] Leitão C, Louro R, Rodrigues DM. Analysis of high temperature plastic behaviour and its relation with weldability in friction stir welding for aluminium alloys AA5083-H111 and AA6082-T6. Mater Des 2012;37:402–9. https://doi.org/10.1016/j.matdes.2012.01.031.